Soils and Rocks
An International Journal of Geotechnical and Geoenvironmental Engineering
www.soilsandrocks.com
ISSN 1980-9743
ISSN-e 2675-5475

Effective stress interpretation of direct simple shear tests using Mohr's circle and finite element analyses

Leonardo De Bona Becker[1#]

Article

Keywords
Direct simple shear
Direct shear
Effective strength
Finite element
Hokksund sand
Mohr's circle

Abstract

The direct simple shear (DSS) test is often employed to assess the undrained strength of fine-grained soils or the liquefaction behavior of coarse soils. Effective strength parameters are not derived from it because the state of stress within the specimen is not considered sufficiently well defined or uniform enough to allow a rigorous interpretation of the results. In the DSS, the failure plane is not imposed, and the principal stresses are not measured, unlike in the direct shear or triaxial tests, respectively. In the past, the DSS was often dismissed because comparisons with other types of tests indicated that it produced lower effective strength parameters. However, this paper presents results of DSS with stacked rings and direct shear tests that are in good agreement with each other. A finite element analysis and Mohr's circle representations are used to assess the internal stresses and strains in the DSS specimen and to locate the failure plane. Based on these results, a reinterpretation of other works is conducted. It is shown that the stress distribution becomes approximately uniform after the early phases of the shearing, and the inclination of the failure plane can be predicted. It is also discussed how the use of low height-to-diameter ratios may influence the results. Thus, the DSS with stacked rings may be considered suitable to determine effective strength and deformability parameters, provided an appropriate height-to-diameter ratio is employed, and the results can be expected to agree with those from other types of tests.

1. Introduction

The interpretation of the Direct Simple Shear test (DSS) results and the factors that affect it has been debated since its introduction and continue to be a matter of research (Mao & Fahey, 2003; Doherty & Fahey, 2011; Wijewickreme et al., 2013; Asadzadeh & Soroush, 2016; Corte et al., 2017; Wai et al., 2022). Despite that, the DSS is routinely used to determine the undrained strength of clays and assess the liquefaction behavior of sands. On the other hand, there is a perception that the effective strength may be underestimated if the DSS is used.

The DSS apparatus was built to simulate in the laboratory the field strain conditions of a thin, horizontal clay layer bounded by sand. That layer is failed by shear deformations (Kjellman, 1951; Bjerrum & Landva, 1966). The objective was to uniformly strain the clay specimen in simple shear and plane strain either in drained or undrained condition. Unlike the triaxial test, in which the stresses may be controlled, the DSS is strain controlled and the direction and magnitude of the principal stresses are unknown. Since the original apparatus was designed for soil specimens with height-to-diameter ratio (H/D) of 0.125, the failure plane was horizontal or almost horizontal because of the constraints imposed by the top and bottom plates. Zekkos et al. (2018) reviewed DSS tests in the literature from 1951 to 2009 and found an average H/D of 0.21.

Later, the DSS has been used to test sands, especially in liquefaction studies (Franke et al., 1979; Silver et al., 1980; Tatsuoka & Silver, 1981; Boulanger & Seed, 1995; Sivathayalan & Ha, 2011; Sadrekarimi, 2020). Moreover, higher H/D ratios have been employed – lower values of H/D would have the disadvantage of hindering the soil tendency to contract or dilate. Thicker samples eliminate that problem. However, the interpretation of the test results becomes more difficult since the failure plane is not readily known, and the principal stresses are ignored. ASTM D6528-17 (ASTM, 2017) defines specifications and procedures for the measurement of constant-volume strength of cohesive soils (including a maximum H/D equal to 0.4) but there is not a standard for sands.

In most DSS tests, only the horizontal displacement (δ_x), the average vertical stress (σ_z) and the average shear stress (τ_{zx}) are measured. The specimen diameter is kept constant by wire or stacked rings. When the specimen height (H) is kept constant, the engineering shear strain (γ_{zx}) is equal to

#Corresponding author. E-mail address: leonardobecker@poli.ufrj.br
[1]Universidade Federal do Rio de Janeiro, Rio de Janeiro, RJ, Brasil.

Submitted on June 18, 2024; Final Acceptance on June 26, 2025; Discussion open until May 31, 2026.
Editor: Renato P. Cunha
https://doi.org/10.28927/SR.2026.005024

δ_x/H and σ_z varies during the shear phase. The actual stress state inside the specimen is unknown since the horizontal stress (σ_x) is not measured. Therefore, only one point of the Mohr's circle is known. For effective stresses, three possible ways to interpret the DSS are shown in Figure 1.

a) The plane of maximum stress obliquity (i.e., the plane of failure – dash-dotted line) is horizontal, and the effective friction angle is given by Equation 1:

$$\phi' = \operatorname{atan}\left(\tau_{zx} / \sigma'_z\right) \quad (1)$$

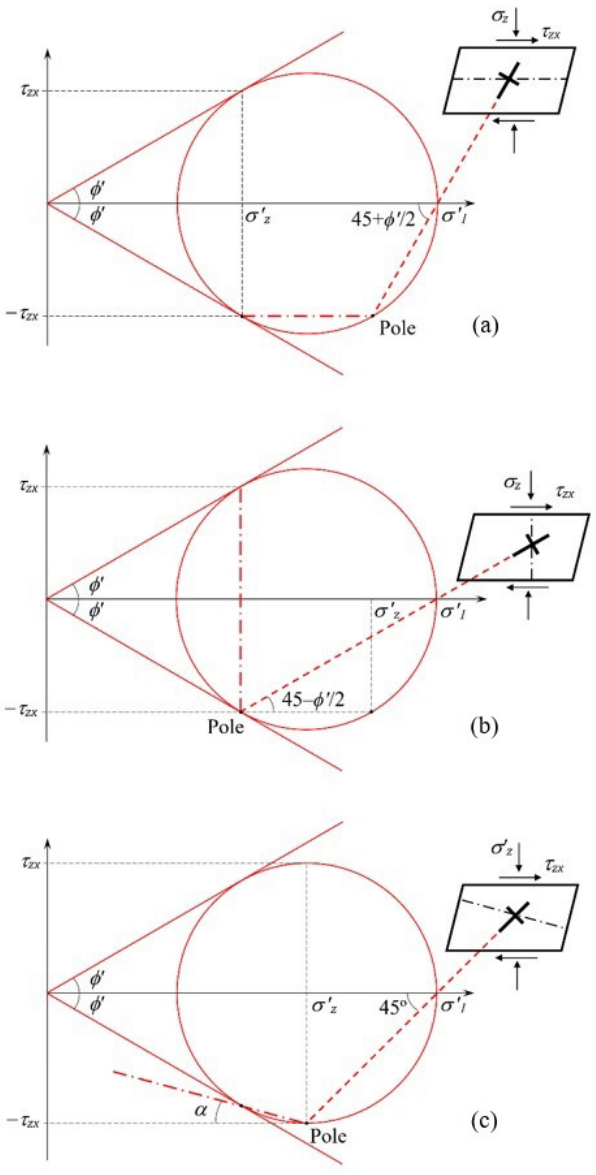

Figure 1. Three interpretations of the DSS test: (a) the failure plane is horizontal; (b) the failure plane is vertical; (c) the horizontal plane is a plane of maximum shear stress (modified from De Josselin de Jong, 1971).

b) De Josselin de Jong (1971) raised the possibility that the sliding plane is vertical, and the effective friction angle is obtained by resolving Equation 2. It is important to note that, according to Equation 2, the maximum value of the τ_{zx}/σ'_z ratio would be approximately 0.35 corresponding to $\phi' = 35°$.

$$\sin\left(\phi'\right)\cdot\cos\left(\phi'\right)/\left[1+\sin^2\left(\phi'\right)\right] = \tau_{zx}/\sigma'_z \quad (2)$$

c) The horizontal plane is a plane of maximum shear stress, and the effective friction angle is given by Equation 3. In this case, the failure plane makes an inclination α with the horizontal.

$$\phi' = \operatorname{asin}\left(\tau_{zx} / \sigma'_z\right) \quad (3)$$

In Figure 1, the major principal plane and the failure plane are represented by dashed and dash-dotted lines, respectively. The crosses represent the orientation of σ'_1 and σ'_3. The horizontal effective stress σ'_x is unknown. The shear stress on the vertical plane is $\tau_{xz} = -\tau_{zx,}$ since the stress field is assumed to be uniform. This assumption becomes reasonable after the initial stages of the shearing, as will be shown below.

In this paper, an analysis of the effective stresses and strains in a constant-volume DSS simulation by the Finite Element Method (FEM) will be presented. The location of the failure plane will be discussed and results of DSS tests in sand and clay will be compared with the FEM analysis.

2. Experimental program

Direct shear (DS) and direct simple shear (DSS) tests were performed with a poorly graded medium sand with angular particles known as Hokksund sand, often used in calibration chamber studies (Parkin & Lunne, 1982; Jamiolkowski et al., 1985). Figure 2 shows the particle size curve and a photograph of the particles along with the tip of a ballpoint pen for size comparison. The maximum and minimum void ratios were determined according to ASTM D4253 (ASTM, 2016a) and ASTM D4254 (ASTM, 2016b) standards ($e_{max} = 0.85$; $e_{min} = 0.52$).

2.1 Direct shear tests (DS)

The direct shear (DS) test was selected to start the experimental program because it resembles a plane strain condition, like the direct simple shear (DSS) test. Three series of six direct shear tests each were performed with remolded samples. The samples were prepared by pluviation after being oven-dried. The samples were not compacted and different densities were obtained by varying the funnel diameter and the drop height. The void ratios after the application of the normal stress were 0.55 ± 0.03, 0.60 ± 0.02, and 0.68 ± 0.02, corresponding to relative densities (D_r) of 96%, 78%, and 54% on average, respectively. The sample dimensions were diameter of 63.5 mm and height of 25 mm.

Soil. Rocks, São Paulo, 2026 49(1):e2026005024

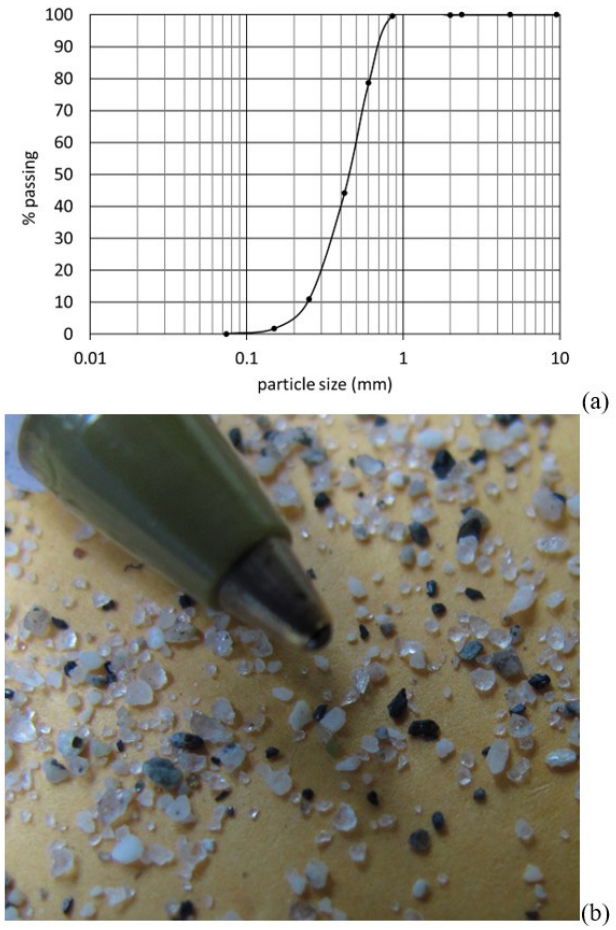

Figure 2. Characteristics of the sand used in this study: (a) particle size analysis; (b) photography of the particles.

Figure 3 presents results of the direct shear tests of the samples with D_r = 96%, typical of dense sands. The results of the looser samples showed less pronounced peaks and less dilatation. Figure 4 presents the shear strength envelopes. The peak friction angle varied from 35° to 45° depending on the initial void ratio. The constant-volume friction angle varied between 32° and 35° (black circles in Figure 4).

2.2 Direct simple shear tests (DSS)

Five constant-volume DSS tests were performed. The samples were prepared using the same remolding procedures outlined above. A servo-controlled mechanism kept the height of the specimens constant by increasing or decreasing the vertical stress. Figure 5 shows the DSS cell, the stacked rings, and the direction of the internal shear stresses that develop on the specimen. Thirty metallic rings coated with Teflon were used to confine the specimens, each with a thickness of 1 mm. The rings rest on metallic bolts depicted by triangles in Figure 5.

The amount of friction is an important boundary condition of the DSS test. Boylan & Long (2009) used a reinforced membrane and assumed that the vertical surface that provides lateral confinement to the specimen is near-frictionless during the whole test. Wai et al. (2022) adopted the same assumption but used stacked rings. When the sample is confined by stacked rings, the near-frictionless assumption is close to reality during the phase of compression by normal stress since the rings are aligned, resulting in a smooth inner surface. However, as the shear strains are applied, this boundary becomes similar to the steps of a staircase, thus providing a highly rough surface that allows the development of the complementary shear stress τ_{xz} (Figure 5b). In the upper left corner of the sample, the rings have freedom to move upward, thus reducing τ_{xz}. However, this movement may be prevented by a support (dashed triangle in Figure 5).

A 0.25 mm-thick unreinforced latex membrane was used, and the dimensions of the specimens were 63 mm in diameter and 30 mm in height (H/D = 0.47). This H/D exceeds the maximum of 0.4 recommended by ASTM D6528-17 (ASTM, 2017) but was chosen to allow a free development of the failure plane as will be shown later. The void ratio after consolidation was 0.55 ± 0.003 (D_r = 91%). The samples were dry, and the shear rate was the same as that employed in the DS tests. Figure 6 shows the variation of shear stress and vertical effective stress during the shear phase of the test. The locus of the (σ'_z, τ_{zx}) pairs of each test is similar to a stress path. Since the volume of the dense sand was kept constant during the shearing, the initial tendency to contract was prevented, and the vertical effective stress was briefly reduced. Later, when the sand would dilate, the constant-volume condition caused a significant increase in the vertical effective stress.

Figure 7 shows the ratio between shear stress and vertical effective stress vs. the engineering shear strain (γ_{zx}). Unlike the DS test, in the DSS test the shear stress curves do not present a clear peak since the dilatation is prevented. The ultimate value of τ_{zx}/σ'_z varies between 0.55 and 0.58 and remains fairly constant after the shear strain reaches 0.15.

Since the specimens were not allowed to dilate in the DSS tests, the comparison considers the constant-volume friction angle developed in the DS tests (Table 1). If one considers the horizontal plane as the failure plane (Equation 1), the effective friction angle in the DSS would range between 29° and 30°. However, this is unlikely since this range is clearly below the constant-volume friction angle obtained in the DS tests. Equation 2 does not have a valid solution because the τ_{zx}/σ'_z ratio exceeds 0.35. Therefore, the failure plane is not vertical. Finally, if one considers the horizontal plane as the plane of maximum shear stress, the effective friction angle would range between 33° and 35° (Equation 3) in the DSS tests, which is in excellent agreement with the DS tests (32-35°).

3. Numerical analysis

A 2D analysis of the results of the DSS test with σ'_z = 100 kPa was conducted using the finite element method (FEM). A mesh study led to the conclusion that 281 triangular elements were adequate to simulate the cross section of the specimen

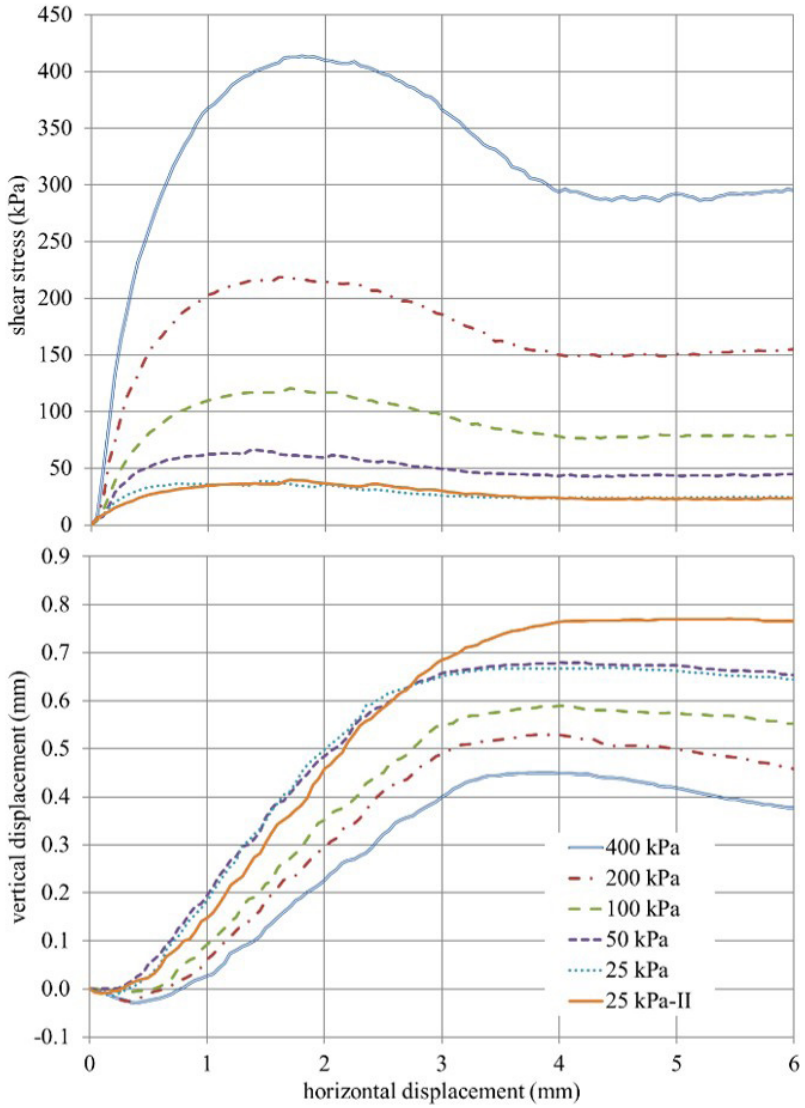

Figure 3. Direct shear test results for D_r = 96%.

Table 1. Effective friction angles of Hokksund (D_r = 54% - 96%).

Test - interpretation	ϕ'_{peak} (°)	ϕ'_{cv} (°)
Direct shear	35 - 45	32 - 35
DSS: ϕ'_{cv} = atan (τ_{zx}/σ'_z)	-	29 - 30
DSS: ϕ'_{cv} = asin (τ_{zx}/σ'_z)	-	33 - 35

(63 mm x 30 mm). The first phase of the analysis simulated the consolidation using a K_0 stress generation process. The subsequent phases simulated the shearing, in which the following boundary conditions were applied (Figure 8):

a) Top boundary: uniform displacement to the right equal to the value measured by the LVDT of the DSS device, and normal stress equal to the vertical force applied by the piston divided by the area of the specimen;

b) Lateral boundaries: variable displacement to the right;

c) Bottom: fixed in the vertical and horizontal directions.

In this FEM analysis, the development of friction on the lateral boundaries was not restricted because of the shape of these boundaries during shear (Figure 5). It should be noted that Wai et al. (2022) compared DSS tests with numerical 3D analyses varying the soil-ring mobilized friction during shearing between zero and $\sigma'_x \cdot \tan\phi'$. They concluded that varying the soil-ring friction during the shearing phase did not affect the measurable stress-strain response. The high soil-ring friction contributed to a uniform state of stress within the specimen. When a frictionless boundary was simulated, complementary shear stresses developed immediately adjacent to vertical boundaries, resulting in a sharp shear stress gradient that transitioned to a uniformly distributed stress state near the center of the specimen (equal to the applied shear stress).

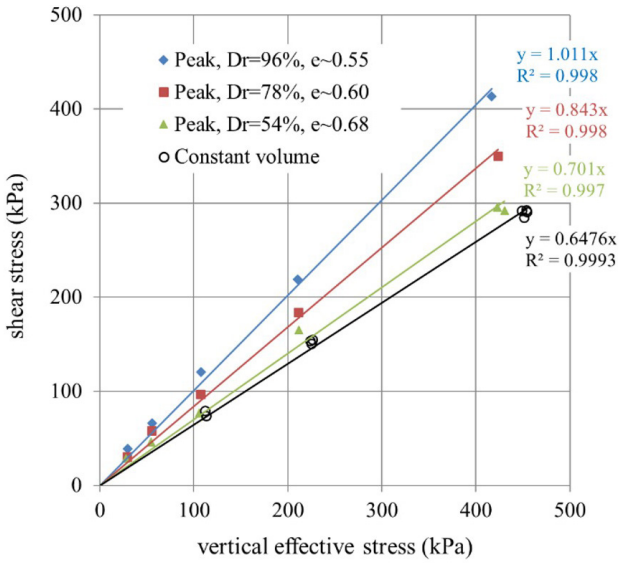

Figure 4. Shear strength envelopes (direct shear tests).

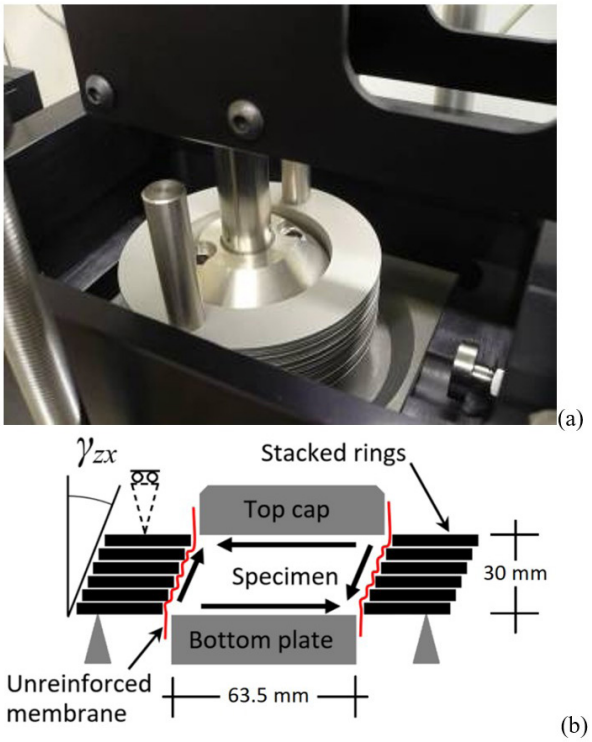

Figure 5. Views of the DSS device: (a) the cell; (b) schematic cross section.

The Hokksund sand was represented in Plaxis by the Hardening Soil Model (Brinkgreve et al., 2006). The properties were defined based on results of direct shear, oedometer, and drained triaxial compression tests (Table 2). These results are in good agreement with the values presented by other authors (Jamiolkowski et al., 1985; Yang et al., 2006; Mazhar, 2009) for similar samples of the same sand.

Table 2. Physical characteristics of Hokksund sand and parameters of the Hardening Soil model.

Parameter	Value	Unit
D_{50}	0.44	mm
C_U	2.1	-
G_s	2.7	-
c'	0	kN/m²
ϕ'_{peak}	45	°
ϕ'_{cv}	33	°
ψ	15	°
K_0	0.29	-
E_{oed}^{ref}	20,600	kN/m²
E_{50}^{ref}	20,600	kN/m²
E_{ur}^{ref}	61,800	kN/m²
m	0.5	-

To validate the FEM analysis, the horizontal force measured by the load cell of the DSS device is compared to the product of the shear stress at the top of the mesh and the area of the specimen (Figure 9) with good agreement.

Figure 10 shows the shear stress distribution at the top of the mesh. Initially, the shear stress varies from left to right, but after phase 6 (i.e., $\gamma_{zx} > 0.42/30 = 1.4\%$) it becomes fairly uniform, as shown by Wai et al. (2022).

Figure 11 shows the principal stresses in several phases of the simulation. At the beginning of the shear phase, the stress field is non-uniform, especially at the lower left corner of the specimen. It is usually considered that the stress state in the DSS is not uniform (e.g., ASTM, 2017). However, the FEM analysis indicates that stress rotation ceases after phase 6, and the stress field becomes approximately uniform, justifying the underlying assumption in Figure 1. Moreover, the inclination of the principal planes with respect to the horizontal is maintained at 45° throughout the whole specimen until the end of the test, regardless of the magnitude of the principal stresses. This result confirms the theoretical deduction made by Oda (1975).

4. Inclination of the failure plane: theoretical analysis and more experimental evidence

The FEM analysis presented herein indicates that the principal stresses increase during the test but the σ'_1/σ'_3 and τ_{zx}/σ'_z ratios become approximately constant after phase 6.

The inclination of the principa planes may be used to estimate the inclination of the failure surface, regardless of the stress magnitudes. The dashed line in Figure 12 has the same inclination as the major principal plane (i.e., 45°) and passes through σ'_1. Thus, it intersects the circle at the pole. Therefore, the pole is the lowest point on the circle. If a horizontal line is drawn through the pole, it must intercept the circle at the point that represents the state of stress on the horizontal plane (point H). Since the pole is the lowest point, the horizontal line must be tangent to the circle and

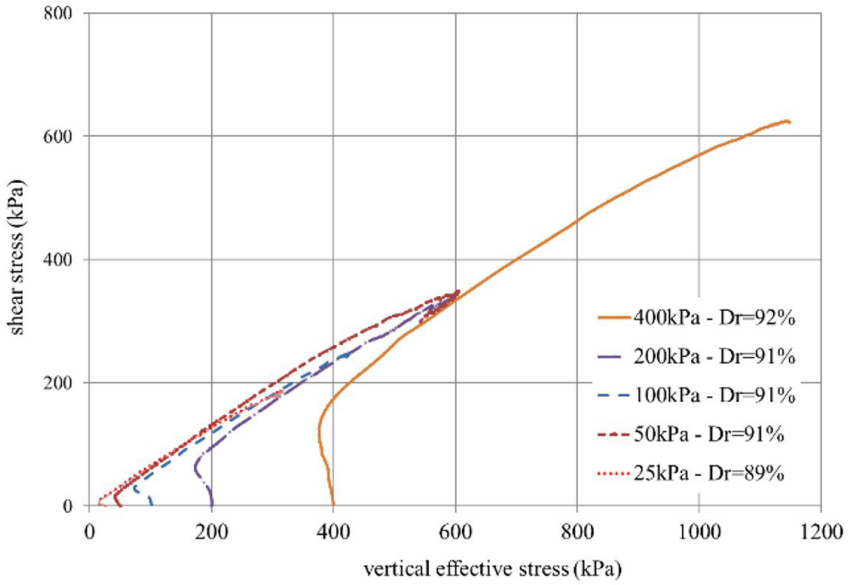

Figure 6. Evolution of the shear and normal stresses acting on the horizontal plane (constant-volume DSS tests).

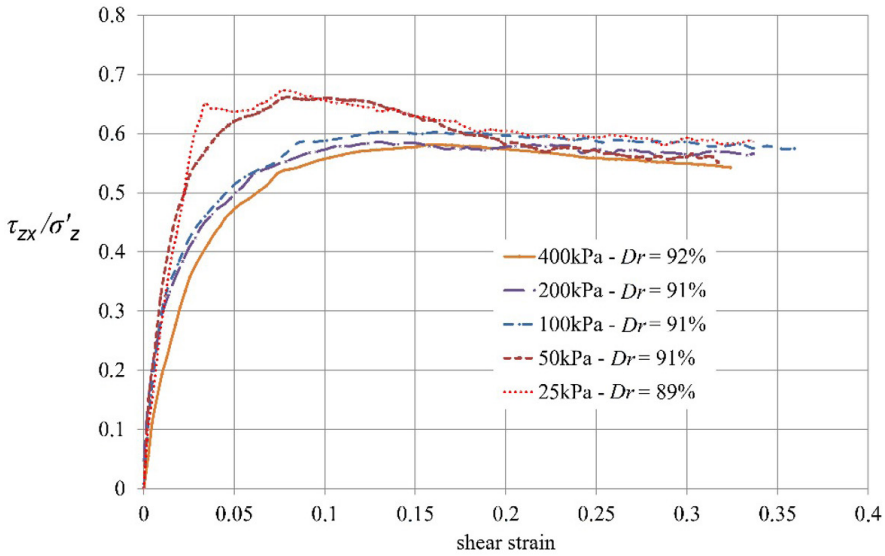

Figure 7. Ratio between the shear stress and the normal effective stress on the horizontal plane (constant-volume DSS tests) vs. shear strain.

H coincides with the pole. This graphical construction confirms the hypothesis that the horizontal plane is the plane of maximum shear stress (Figure 1c). Asadzadeh & Soroush (2016) reached a similar conclusion by means of discrete element method (DEM) simulation of DSS tests with glass beads.

Point F represents the state of stress on the failure plane. The constant-volume friction angle is ϕ'_{cv}. Since H is the pole, the line segment FH is parallel to the failure plane. Let α be the angle between the failure plane and the horizontal. Because θ, β, and ϕ'_{cv} are internal angles of triangle OFH, it follows that $\theta + \beta + \phi'_{cv} = 180°$. As triangle OFH is isosceles, $\theta = \beta$, and therefore, $\theta = 90 - \phi'_{cv}/2$. Furthermore, considering the angles adjacent to point F, it follows that $\phi'_{cv} + (\theta - \alpha) = 90°$. Thus, the inclination of the failure plane is given by:

$$\alpha = \phi' cv / 2 \quad (4)$$

This theoretical conclusion based on Mohr's circle is in agreement with numerical analyses performed by Doherty & Fahey (2011) and Wijewickreme et al. (2013). In the first work, a modified Cam-clay soil model was used in a 3D FEM analysis to simulate a DSS under constant-volume plane-strain simple-shear conditions. In the second work,

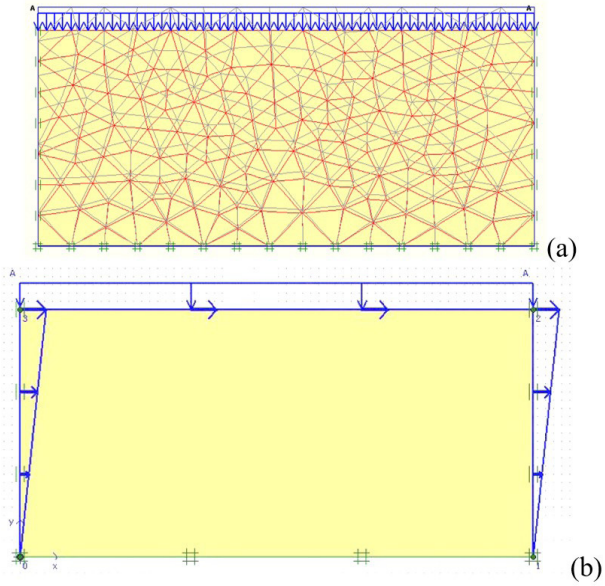

Figure 8. FEM analysis of the DSS test: (a) deformed mesh at the end of the consolidation phase; (b) boundary conditions of the shearing phases.

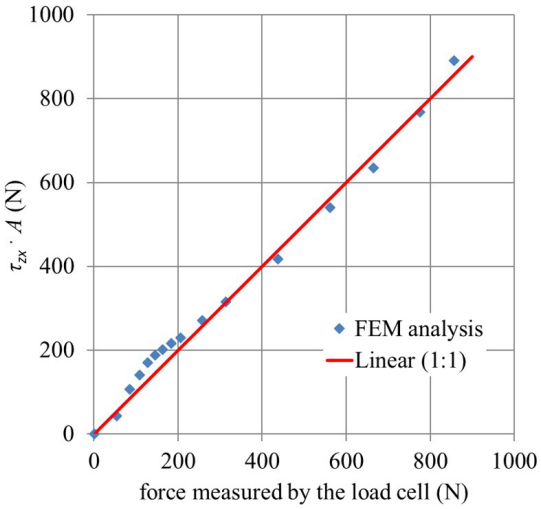

Figure 9. Comparison between horizontal force measured in the DSS test and estimated by the FEM analysis.

DEM simulations of a theoretical DSS test reached the same conclusion as Equation 4, at the peak mobilized friction angle. However, Wijewickreme et al. (2013) concluded that, after large shear strains in the constant-volume test, the failure planes would rotate, and the horizontal plane seemed to be a plane of maximum stress obliquity. This continuous stress rotation is not in agreement with the numerical simulation presented herein (Figure 11). Also, the DSS results do not support a continuous stress rotation since the ratio between shear and normal stresses measured in the horizontal plane remains approximately constant for $\gamma_{zx} > 0.15$ (Figure 7).

Moreover, Grognet (2011), den Haan & Grognet (2014) developed a unique large-sized experimental direct simple shear test device with transparent sides that permitted the visualization of the failure plane. They tested soil samples at low normal stress ($\sigma'_z \sim 5$ kPa). The boundary conditions of their "Test 2" were similar to the configuration used in the experimental program presented herein, with a height over length ratio (H/L) equal to 0.51 and strips that slide on top of each other confining the sides of the sample, like the stacked rings. The soil was a remolded clay from Oostvaardersplassen park in the Netherlands (OVP). The

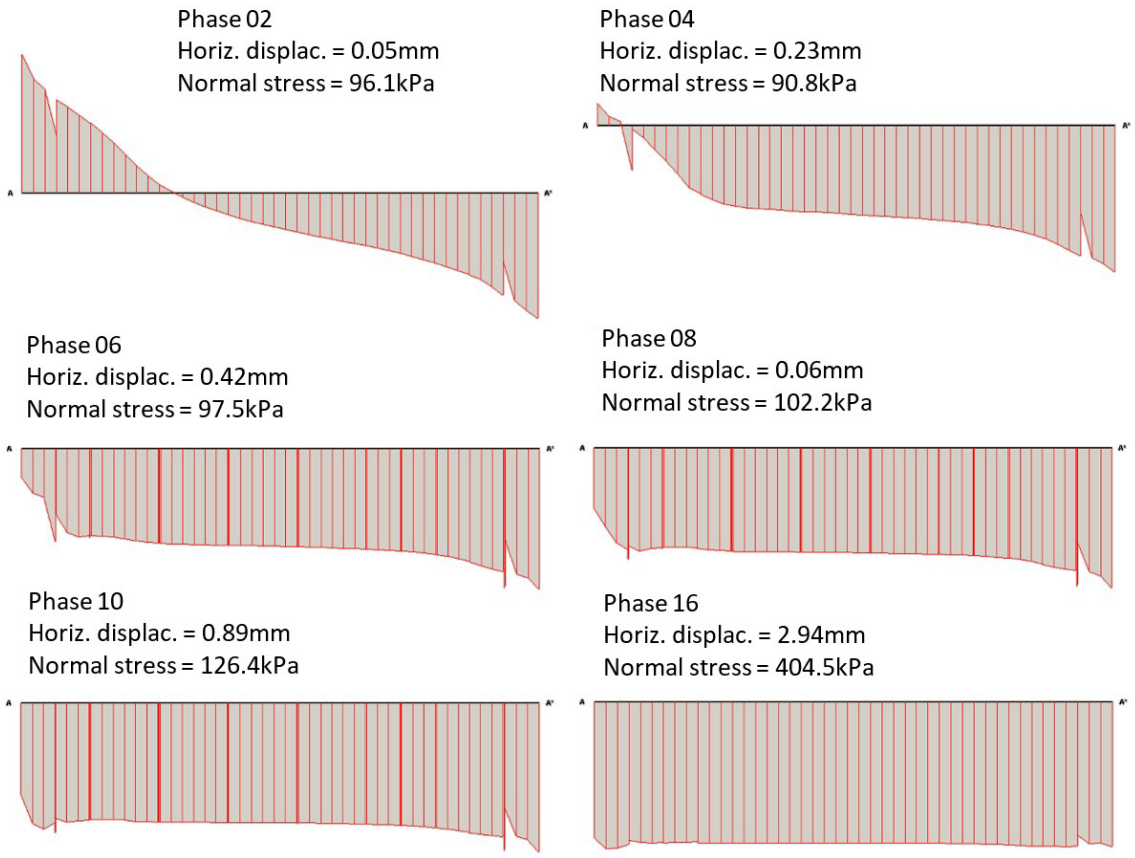

Figure 10. FEM simulation: shear stress at the top boundary of the mesh at distinct phases.

shear rate was low enough to avoid the buildup of pore pressure excess. Figure 13 shows the vertical cross section in the middle of the specimen after the test. Shear planes with an inclination ranging from 16° to 22° to the horizontal are clearly visible. Since the photo shows that the failure plane is neither horizontal nor vertical, interpretations based on Equation 1, Equation 2, and Figures 1a and 1b are not valid.

According to Equation 4, the inclination of the failure planes in Figure 13 indicates that $\phi' = 32°$ to 44° for the tested clay at low stresses. This is a high friction angle range for a clay, but OVP has an unusually high ϕ' owing to the peculiarities of its multi-level organic fabric. Cheng et al. (2007) reported $\phi' = 38°$ to 46° at low confining stresses.

The same concept may be applied to undrained DSS tests, provided the critical state is considered. Zekkos et al. (2018) developed a large-size DSS (maximum $H/D = 0.45$) and compared their results with conventional-sized DSS devices using Ottawa sand C109. Figure 14a shows four tests with this sand (where the dashed and the continuous lines indicate tests with the conventional and the large-size devices, respectively). The bold dashed line represents a strength envelope with an apparent inclination of 0.5. This corresponds to $\phi'_{cv} = \arcsin 0.5 = 30°$ (Equation 3), in excellent agreement with the constant-volume friction angle of this sand as 29.8° reported by Wijewickreme (1982) and Sasitharan et al. (1994). Morgenstern et al. (2016) used 15 triaxial tests (CIU, CID, CAU types) to determine the critical state friction angle of the sand tailings from the Fundão Dam in Mariana Brazil ($\phi'_{cs} = 33°$). DSS undrained tests in the same material were also performed (Figure 14b). At the critical state, the τ_{zx}/σ'_z ratio is equal to 0.55 (dashed line) which corresponds to $\phi'_{cs} = \text{asin } 0.55 = 33°$.

Another consequence of Equation 4 is that a specimen with a low H/D ratio will not have enough height to allow for the complete development of the failure plane, thus altering the results. For example, a soil with $\phi'_{cv} = 30°$ would require $H/D > \tan 15° = 0.27$. In the past, H/D ratios were frequently low (e.g. $H/D = 0.125$ in Bjerrum & Landva (1966) and 0.2 in Budhu & Britto (1987)). This may have been the reason why comparisons of DSS test results with results from other devices like the triaxial and the hollow cylinder led to the conclusion that the DSS produces unreliable soil strengths (Saada & Townsend, 1981). Therefore, a high H/D is important to ensure that the top and bottom do not interfere with the development of the failure plane. For instance, Morgenstern et al. (2016) used $H/D = 0.3$. Coincidentally, according to the Equation 4, this is the lower limit for a soil with $\phi'_{cs} = 33°$ since a test with $H/D < 0.3$ would result in the top and bottom restraining the development of the failure plane.

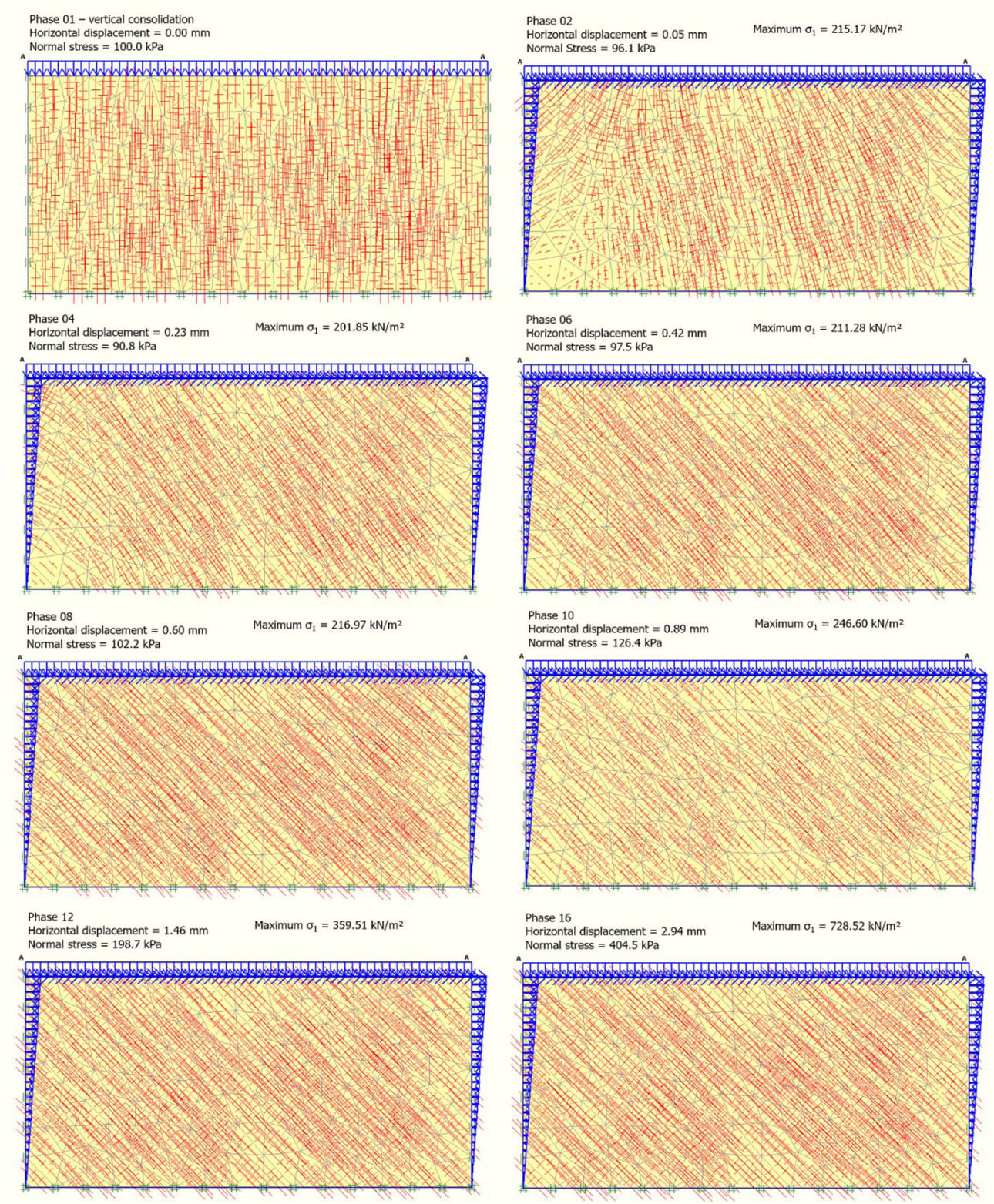

Figure 11. FEM simulation: principal stresses at distinct phases.

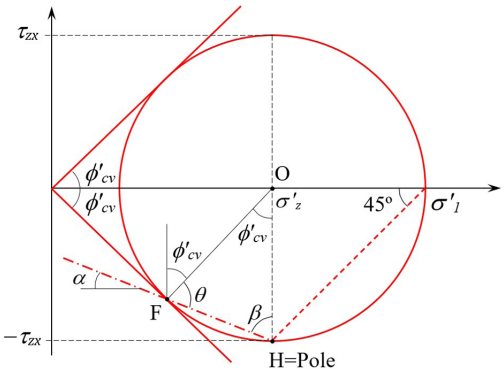

Figure 12. Mohr's circle of stress of the constant-volume DSS test.

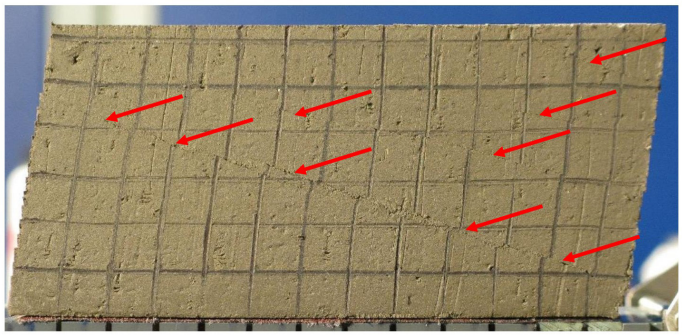

Figure 13. Results from a simple shear test on OVP clay sample (γ = 20%) at the middle vertical plane (adapted from Grognet, 2011).

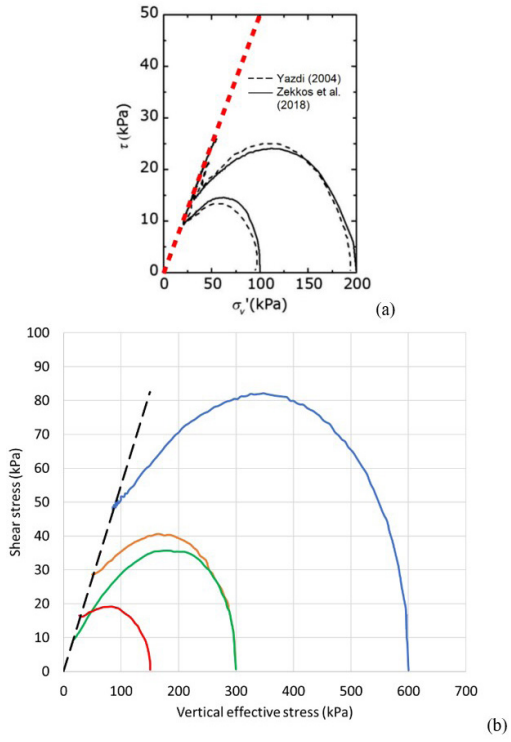

Figure 14. Results from undrained DSS tests: (a) Ottawa C 109 sand (adapted from Zekkos et al., 2018); (b) Fundão sand tailings (redrawn from Morgenstern et al., 2016).

5. Conclusions

Two-dimensional finite element (FEM) analysis and experimental results from constant-volume high height-to-diameter (H/D) ratio DSS tests using stacked rings showed good agreement and indicated the following:

a) The stress field in the DSS specimen became approximately uniform after the initial stages of shearing, unlike the assumption stated in ASTM D6528-17 (ASTM, 2017) for low H/D ratio specimens;
b) The principal stress planes were observed at an inclination of 45°, as predicted by Oda (1975);
c) Although the principal stresses varied throughout the test, their ratio and orientation became constant after the initial stages.

As a result of the stress uniformity in the specimen, a Mohr's circle-based analysis is valid. Given that the principal planes are inclined at 45°, the stress analysis presented herein demonstrates that the horizontal plane is the plane of maximum shear stress, and that the inclination of the failure plane equals $\phi'_{cv}/2$.

Therefore, constant-volume DSS tests with stacked rings can be used to determine the constant-volume friction angle using the equation $\phi'_{cv} = \arcsin(\tau_{zx}/\sigma'_z)$, provided that an appropriate H/D ratio is selected.

Further testing is needed to assess the influence of the H/D ratio on the results. However, the limit recommended by ASTM D6528-17 (ASTM, 2017) ($H/D \leq 0.4$) may not be suitable for all soils. For instance, an $H/D = 0.25$ would be inadequate for soils with $\phi'_{cv} > 28°$, as the top and bottom boundaries would constrain the development of the failure surface. This is because the theoretical inclination of the failure plane was shown to be equal to $\phi'_{cv}/2$. On the other hand, an $H/D = 0.4$ would be suitable for all soils with ϕ'_{cv} less than or equal to 43°.

Acknowledgements

The author would like to thank Prof. Vitor Aguiar for the invaluable suggestions and comments, Prof. Fernando Danziger for the use of the DSS, Mr. André Q. Bastos and Mr. George L. Teles for the execution of the tests, and PIBIC/CNPq/UFRJ program for their scholarship.

Declaration of interest

The author has no conflicts of interest to declare. The author has observed and affirmed the contents of the paper and there is no financial interest to report.

Data availability

All data produced or examined in the course of the current study are included in this article.

Declaration of use of Generative Artificial Intelligence

This work was prepared without the assistance of Generative Artificial Intelligence (GenAI).

List of symbols and abbreviations

c'	Effective cohesion
e_{max}	Maximum void ratio
e_{min}	Minimum void ratio
m	Stress dependent stiffness of the Hardening Soil model (power law)
C_U	Uniformity coefficient
D	Diameter of the DSS specimen
D_r	Relative density
D_{50}	Particle size at which 50% of soil is finer
E_{50}^{ref}	Secant modulus at 50% of the failure deviatoric stress for a reference stress p'
E_{oed}^{ref}	Secant modulus for a reference stress p' (oedometer test)
E_{ur}^{ref}	Secant modulus for a reference stress p' (unloading and reloading)
G_s	Specific gravity of solids
H	Height of the DSS specimen
K_0	At rest earth pressure coefficient
α	Inclination of the failure plane with the horizontal
γ_{zx}	Engineering shear strain
δ_x	Horizontal displacement
$\sigma'_{1,3}$	Principal effective stresses
σ_x	Average horizontal stress
σ'_z	Average vertical effective stress
σ_z	Average vertical stress
τ_{zx}	Average shear stress on the horizontal plane
ϕ'	Effective friction angle
ϕ'_{cs}	Critical state friction angle
ϕ'_{cv}	Constant-volume friction angle
ϕ'_{peak}	Peak friction angle
ψ	Dilatation angle

References

Asadzadeh, M., & Soroush, A. (2016). Fundamental investigation of constant stress simple shear test using DEM. *Powder Technology*, 292, 129-139. http://doi.org/10.1016/j.powtec.2016.01.029.

ASTM D4253-16. (2016a). *Standard test methods for maximum index density and unit weight of soils using a vibratory table.* ASTM International, West Conshohocken, PA. http://doi.org/10.1520/D4253-16E01.

ASTM D4254-16. (2016b). *Standard test methods for minimum index density and unit weight of soils and calculation of relative density.* ASTM International, West Conshohocken, PA. http://doi.org/10.1520/D4254-16.

ASTM D6528-17. (2017). *Standard test method for consolidated undrained direct simple shear testing of fine grain soils.* ASTM International, West Conshohocken, PA. http://doi.org/10.1520/D6528-17.

Bjerrum, L., & Landva, A. (1966). Direct simple-shear tests on a Norwegian quick clay. *Geotechnique*, 16(1), 1-20. http://doi.org/10.1680/geot.1966.16.1.1.

Boulanger, R.W., & Seed, R.B. (1995). Liquefaction of sand under bidirectional monotonic and cyclic loading. *Journal of Geotechnical Engineering*, 121(12), 870-878. http://doi.org/10.1061/(ASCE)0733-9410(1995)121:12(870).

Boylan, N., & Long, M.M. (2009). Development of a direct simple shear apparatus for peat. *Geotechnical Testing Journal*, 32(2), 126-138. http://doi.org/10.1520/GTJ101703.

Brinkgreve, R.B.J., Broere, W., & Waterman, D. (2006). *Plaxis 2D version 8.* Delft: Plaxis B.V.

Budhu, M., & Britto, A. (1987). Numerical analysis of soils in simple shear devices. *Soil and Foundation*, 27(2), 31-41. http://doi.org/10.3208/sandf1972.27.2_31.

Cheng, X.H., Ngan-Tillard, D.J.M., & Den Haan, E.J. (2007). The causes of the high friction angle of Dutch organic soils. *Engineering Geology*, 93(1-2), 31-44. http://doi.org/10.1016/j.enggeo.2007.03.009.

Corte, M.B., Festugato, L., & Consoli, N.C. (2017). Development of a cyclic simple shear apparatus. *Soils and Rocks*, 40(3), 279-289. http://doi.org/10.28927/SR.403279.

De Josselin de Jong, G. (1971). Discussion on stress-strain behavior of soils. In *Proceedings of the Roscoe Memorial Symposium* (pp. 258-261). Cambridge: Foulis.

den Haan, E.J., & Grognet, M. (2014). A large direct simple shear device for the testing of peat at low stresses. *Géotechnique Letters*, 4(4), 283-288. http://doi.org/10.1680/geolett.14.00033.

Doherty, J., & Fahey, M. (2011). Three-dimensional finite element analysis of the direct simple shear test. *Computers and Geotechnics*, 38(7), 917-924. http://doi.org/10.1016/j.compgeo.2011.05.005.

Franke, E., Kiekbusch, M., & Schuppener, B. (1979). A new direct simple shear device. *Geotechnical Testing Journal*, 2(4), 190-199. http://doi.org/10.1520/GTJ10457J.

Grognet, M. (2011). *The boundary conditions in direct simple shear tests, development for peat testing at low vertical stress* [Master's dissertation]. Delft University of Technology. Retrieved in June 18, 2024, from http://web.archive.org/web/20200720111535/https://repository.tudelft.nl/islandora/object/uuid:c320f947-6a68-4e8b-830a-b94b88d3e43f?collection=education

Jamiolkowski, M., Baldi, G., Bellotti, R., Ghionna, V., & Pasqualini, E. (1985). Penetration resistance and liquefaction of sands. In *Proceedings of the XI International Conference on Soil Mechanics and Foundation Engineering* (Vol. 4, pp. 1891-1896), San Francisco, CA. Retrieved in June 18, 2024, from https://www.issmge.org/publications/publication/penetration-resistance-and-liquefaction-of-sands

Kjellman, W. (1951). Testing the shear strength of clay in Sweden. *Geotechnique*, 2(3), 225-232. http://doi.org/10.1680/geot.1951.2.3.225.

Mao, X., & Fahey, M. (2003). Behaviour of calcareous soils in undrained cyclic simple shear. *Geotechnique*, 53(8), 715-727. http://doi.org/10.1680/geot.2003.53.8.715.

Mazhar, M.A. (2009). *Properties of a sand to be used in a NUMGE 2010 model test* [Master's dissertation]. Norwegian University of Science and Technology, Trondheim.

Morgenstern, N.R., Vick, S.G., Viotti, C.B., & Watts, B.D. (2016). *Fundão tailings dam review panel report on the immediate causes of the failure of the Fundão dam*. New York: Cleary Gottlieb Steen & Hamilton LLP.

Oda, M. (1975). On the relation $\tau/\sigma_N = \kappa \cdot \tan \psi$ in the simple shear test. *Soil and Foundation*, 15(4), 35-41. http://doi.org/10.3208/sandf1972.15.4_35.

Parkin, A.K., Lunne, T. (1982). *Boundary effects in the laboratory calibration of a cone penetrometer for sand* (Norwegian Geotechnical Institute Publication, No. 138). Oslo: Norwegian Geotechnical Institute.

Saada, A.S., & Townsend, F.C. (1981). State of the art: laboratory strength testing of soils. In R.N. Yong & F.C. Townsend (Eds.), *Laboratory shear strength of soil* (pp. 7-77). West Conshohocken: ASTM International. http://doi.org/10.1520/STP28744S.

Sadrekarimi, A. (2020). Forewarning of Static Liquefaction Landslides. *Journal of Geotechnical and Geoenvironmental Engineering*, 146(9), 04020090. http://doi.org/10.1061/(ASCE)GT.1943-5606.0002320.

Sasitharan, S., Robertson, P.K., Sego, D.C., & Morgenstern, N.R. (1994). State boundary surface for very loose sand and its practical implications. *Canadian Geotechnical Journal*, 31(3), 321-334. http://doi.org/10.1139/t94-040.

Silver, M.L., Tatsuoka, F., Phukunhaphan, A., & Avramidis, A.S. (1980). Cyclic undrained strength of sand by triaxial and simple shear test. In *Proceedings of the Specialty Conference on Earthquake Engineering and Soil Dynamics* (Vol. 3, pp. 1478-1481), Pasadena, CA. Reston: ASCE. Retrieved in June 18, 2024, from http://web.archive.org/web/20160109122330/https://www.iitk.ac.in/nicee/wcee/article/7_vol3_281.pdf

Sivathayalan, S., & Ha, D. (2011). Effect of static shear stress on the cyclic resistance of sands in simple shear loading. *Canadian Geotechnical Journal*, 48(10), 1471-1484. http://doi.org/10.1139/t11-056.

Tatsuoka, F., & Silver, M. (1981). Undrained stress-strain behavior of sand under irregular loading. *Soil and Foundation*, 21(1), 51-66. http://doi.org/10.3208/sandf1972.21.51.

Wai, D., Manmatharajan, M.V., & Ghafghazi, M. (2022). Effects of imperfect simple shear test boundary conditions on monotonic and cyclic measurements in sand. *Journal of Geotechnical and Geoenvironmental Engineering*, 148(1), 04021164. http://doi.org/10.1061/(ASCE)GT.1943-5606.0002682.

Wijewickreme, D. (1982). *Constant volume friction angle of granular materials* [Master's dissertation]. The University of British Columbia, Vancouver. Retrieved in June 18, 2024, from http://web.archive.org/web/20200219045605/https://open.library.ubc.ca/media/download/pdf/831/1.0062924/2

Wijewickreme, D., Dabeet, A., & Byrne, P. (2013). Some observations on the state of stress in the direct simple shear test using 3D discrete element analysis. *Geotechnical Testing Journal*, 36(2), 292-299. http://doi.org/10.1520/GTJ20120066.

Yang, S., Lacasse, S., & Sandven, R. (2006). Determination of the transitional fines content of mixtures of sand and non-plastic fines. *Geotechnical Testing Journal*, 29(2), 102-107. http://doi.org/10.1520/GTJ14010.

Zekkos, D., Athanasopoulos-Zekkos, A., Hubler, J., Fei, X., Zehtab, K.H., & Marr, W.A. (2018). Development of a large-size cyclic direct simple shear device for characterization of ground materials with oversized particles. *Geotechnical Testing Journal*, 41(2), 263-279. http://doi.org/10.1520/GTJ20160271.